




Few-cycle vortex beam generated from self-compression of midinfrared femtosecond vortices in thin plates

Litong Xu ¹, Dongwei Li,² Junwei Chang,² Tingting Xi ^{1,*} and Zuoqiang Hao ^{2,†}

¹*School of Physical Sciences, University of Chinese Academy of Sciences, Beijing 100049, China*

²*Shandong Provincial Engineering and Technical Center of Light Manipulations and Shandong Provincial Key Laboratory of Optics and Photonic Device, School of Physics and Electronics, Shandong Normal University, Jinan 250358, China*



(Received 4 July 2022; accepted 7 November 2022; published 22 November 2022)

We demonstrate theoretically that a few-cycle vortex beam with high peak power can be generated by self-compression of a midinfrared femtosecond vortex beam in thin fused silica plates. We first investigate the requirements of solitonlike pulse self-compression of the vortex beam on a laser wavelength and parameters of the thin plates based on three preconditions of sufficient spectral broadening, appropriate dispersion compensation, and inhibition of multiple filamentation. Our simulations confirm the existence of the solitonlike pulse self-compression regime of the vortex beam and demonstrate that the 3- μm femtosecond vortex beam with an input duration of 90 fs can be compressed to 15.1 fs with the vortex characteristics preserved. The conversion efficiency is as high as 91.5%, and the peak power reaches 0.18 TW. Our work is instructive for experiments generating high-peak-power few-cycle vortex beams and will help with obtaining isolated attosecond light vortices, opening an alternative perspective in ultrafast science.

DOI: [10.1103/PhysRevA.106.053516](https://doi.org/10.1103/PhysRevA.106.053516)

I. INTRODUCTION

Vortex beams have been widely studied in the last few decades for both the intriguing physics involved and potential applications [1]. The orbital angular momentum (OAM) induced by the helical phase wave front connects the classical and quantum physics, offering a convenient tool to study quantum information and quantum computation [2]. It also provides a new freedom to influence light-matter interactions, facilitating atom trapping and guiding [3]. When the OAM is introduced to ultrashort pulses, more fascinating phenomena arise in the nonlinear propagation, such as spatiotemporal vortices [4], vortex algebra [5], and orbital-to-spin angular momentum conversion [6]. One of the most attractive topics concerning femtosecond vortex beams is high-harmonic generation (HHG), which is an effective tool to generate extreme-ultraviolet vortex beams [7–10] and trains of attosecond light vortices [11]. The attosecond light vortices can provide unique light sources for the fundamental study of and diagnostic tools for ultrafast science [12]. For example, attosecond light vortices can trigger transitions forbidden by selection rules [13,14] and facilitate probing molecular chirality on a subfemtosecond timescale [15]. For reliable generation of isolated attosecond light vortices, high-power few-cycle vortex beams are necessary [16], which may also be useful for the generation of vortex beams in the terahertz regime [17]. However, to the best of our knowledge, only few-cycle vortex beams with gigawatt-level peak power have been generated via optical parametric amplification [18].

Although obtaining an intense midinfrared (MIR) few-cycle vortex beam via a plasma-based photon decelerator driven by a vortex beam in underdense plasma has been proposed theoretically [19], the energy-conversion efficiency is relatively low, and the experiment conditions may not be commonly available.

Actually, it is intuitive to obtain few-cycle vortex beams by postcompression of supercontinuum vortices, which have been realized using the four-wave frequency-mixing approach [5] and the thin-plate scheme [20]. However, the postcompression of these supercontinuum vortices will cause inevitable energy loss [21]. As an alternative method, self-compression is of particular interest because of its convenience for generating few-cycle pulses with high conversion efficiency [22,23]. Although it is well known that self-compression may occur when intense MIR femtosecond pulses propagate in media with anomalous dispersion, self-compression of femtosecond vortex beams has not been studied. This is because the strong nonlinear effects and initial noise usually lead to multiple filamentation, which will destroy the vortex characteristics of the initial beam [24]. The study of MIR few-cycle vortex beams will be helpful for the generation of isolated and shorter attosecond vortices with higher photon energy [25,26]. To generate high-power few-cycle MIR vortex beams, the thin-plate scheme is a promising candidate for performing pulse self-compression of the MIR femtosecond vortex beam while avoiding multiple filamentation [27,28]. With the thin-plate setup, a femtosecond pulse with a central wavelength of 4 μm was self-compressed to 29.4 fs with a high efficiency [29]. Moreover, this scheme was applied to obtain powerful supercontinuum vortices in the near-infrared regime [20]. However, it is unknown whether the MIR femtosecond vortex beam can be self-compressed to a few-cycle vortex beam with high

*ttxi@ucas.ac.cn

†zqhao@sdu.edu.cn

peak power. Further study is highly anticipated because the complicated spatiotemporal requirements, including sufficient spectral broadening, appropriate negative-dispersion compensation, and inhibition of destructive interference of multiple filaments, need to be simultaneously satisfied.

In this paper, we first theoretically investigate the conditions for obtaining few-cycle vortex beams via pulse self-compression in thin plates. Based on the spatiotemporal requirements for generating high-power few-cycle vortex beams, we give the criteria for choosing the laser wavelength, as well as the parameters of the plates. Then we confirm the theoretical approximation with simulations and show the successful generation of a MIR few-cycle vortex beam with high peak power by self-compression of a 3- μm femtosecond vortex beam. In this case, the vortex pulse is successfully compressed from 90 to 15.1 fs, with the initial vortex phase distribution preserved. The solitonlike self-compression generated by using this scheme leads to a very high conversion efficiency and compression ratio. The results demonstrate that this scheme satisfies the complex spatiotemporal requirements for generating high-peak-power few-cycle vortex beams, for which spectrum broadening, dispersion compensation, and inhibition of multiple filamentation can be realized simultaneously. Our work provides important guidance for the experiment, and the generation of high-power few-cycle vortex beams will help with obtaining isolated attosecond light vortices, opening an alternative perspective in ultrafast science.

II. THEORY AND ANALYSIS

To obtain few-cycle pulses, we need a superbroadened spectrum and strong negative dispersion that can compensate for the positive chirp induced by self-phase modulation (SPM). In addition, to maintain the vortex characteristics, multiple filamentation should be avoided. Based on the above considerations, we propose three criteria for choosing the parameters of the thin plates, as well as the laser wavelength.

(1) The thickness of the plate L should be larger than the nonlinear length l_{nl} to trigger supercontinuum generation and smaller than the characteristic length for multiple filamentation l_m to maintain the vortex phase:

$$l_{\text{nl}} < L < l_m. \quad (1)$$

Here $l_{\text{nl}} = 1/k_0 n_2 I_0$, k_0 is the central wave number, n_2 is the coefficient of the nonlinear refractive index, and I_0 is the incident intensity. According to previous studies [28,30], the typical length scale for spatial modulation instability to build up (the onset of multiple filamentation) l_m is about $5l_{\text{nl}}$. The inequality (1) gives the condition that enables us to broaden the spectrum of femtosecond vortices with the vortex characteristics preserved.

(2) For pulse self-compression via anomalous dispersion, the group-delay dispersion (GDD) induced by the material should surpass that induced by SPM:

$$|k^{(2)}|L > \varphi''_{\text{out}}, \quad (2)$$

where $k^{(2)}$ is the group-velocity-dispersion coefficient. Consider a chirp-free pulse with duration τ_0 and central wavelength λ_0 injected into a fused silica plate; the GDD rising

from SPM is given by [29]

$$\varphi''_{\text{out}} = \frac{\tau_0^2 B}{2 \ln 2(1 + 4B^2)}, \quad (3)$$

where the nonlinear phase shift $B = k_0 n_2 I_0 L = L/l_{\text{nl}}$. This condition ensures the solitonlike pulse self-compression.

(3) In order to obtain a few-cycle pulse with the vortex characteristics preserved, the typical compression length for reaching the minimum pulse duration l_c should be smaller than the characteristic length for multiple filamentation l_m :

$$l_c < l_m. \quad (4)$$

The compression length can be approximated by [31]

$$l_c \approx \frac{\pi}{2} (0.32 \sqrt{l_d l_{\text{nl}}} + 1.1 l_{\text{nl}}), \quad (5)$$

where l_d is the dispersion length:

$$l_d = (\tau_0/1.665)^2 / |k^{(2)}|. \quad (6)$$

Based on the three criteria above, we obtain the condition for the generation of a MIR few-cycle vortex beam, which is written as

$$\eta = \frac{18.4 |k^{(2)}| \lambda_0}{n_2 I_0 \tau_0^2} - 1 > 0. \quad (7)$$

In the above formula, n_2 is fixed at $2 \times 10^{-16} \text{ cm}^2/\text{W}$ because its dispersion in the midinfrared range is negligible [32]. I_0 is assumed to be larger than $10 \text{ TW}/\text{cm}^2$ for efficient spectrum broadening and lower than $20 \text{ TW}/\text{cm}^2$ to avoid damage to fused silica [28]. This can be achieved by adjusting the spacings of the plates. We set the initial pulse duration to be nine optical cycles, namely, $\tau_0 = 9\lambda_0/c$. When using the above settings, we can draw the evolution curve of η against λ_0 , as shown in Fig. 1(a). As indicated by the red dashed line, solitonlike pulse compression of the femtosecond vortex beam requires that the laser wavelength be $\lambda_0 > 2.48 \mu\text{m}$.

As a check on this, we performed simulations using wavelengths of 2, 2.5, and 3 μm . The propagation of the femtosecond vortex beam in the thin-plate scheme can be described by the generalized nonlinear envelope equation coupled with the electron-density equation [33], which can describe the evolution of laser pulses with a duration down to a single optical cycle. The coupled equations are written as

$$\begin{aligned} \frac{\partial E}{\partial z} = & \frac{i}{2k_0} T^{-1} \nabla_{\perp} E + \frac{i\omega_0}{c} n_2 T \int_{-\infty}^t \mathcal{R}(t-t') |E(t')|^2 dt' E \\ & + i\widehat{D}E - \frac{ik_0}{2n_0^2 \rho_c} T^{-1} \rho E - \frac{U_i W(|E|)}{2|E|^2} (\rho_{\text{nt}} - \rho) E, \end{aligned} \quad (8)$$

$$\frac{\partial \rho}{\partial t} = W(|E|) (\rho_{\text{nt}} - \rho) - \frac{\rho}{\tau_{\text{rec}}}. \quad (9)$$

The terms on the right side of Eq. (8) account for diffraction, the optical Kerr effect, dispersion, plasma defocusing, and ionization loss, respectively. k_0 is the corresponding wave number of the central wavelength λ_0 . The operator $T = 1 + i\partial_t/\omega_0$ is responsible for space-time focusing before the diffraction term and self-steepening before the Kerr term [34]. The coefficient of the nonlinear refractive index n_2 is taken to be $2 \times 10^{-16} \text{ cm}^2/\text{W}$ for fused silica [32] and $1 \times 10^{-19} \text{ cm}^2/\text{W}$ for air [20]. The nonlinear Kerr response

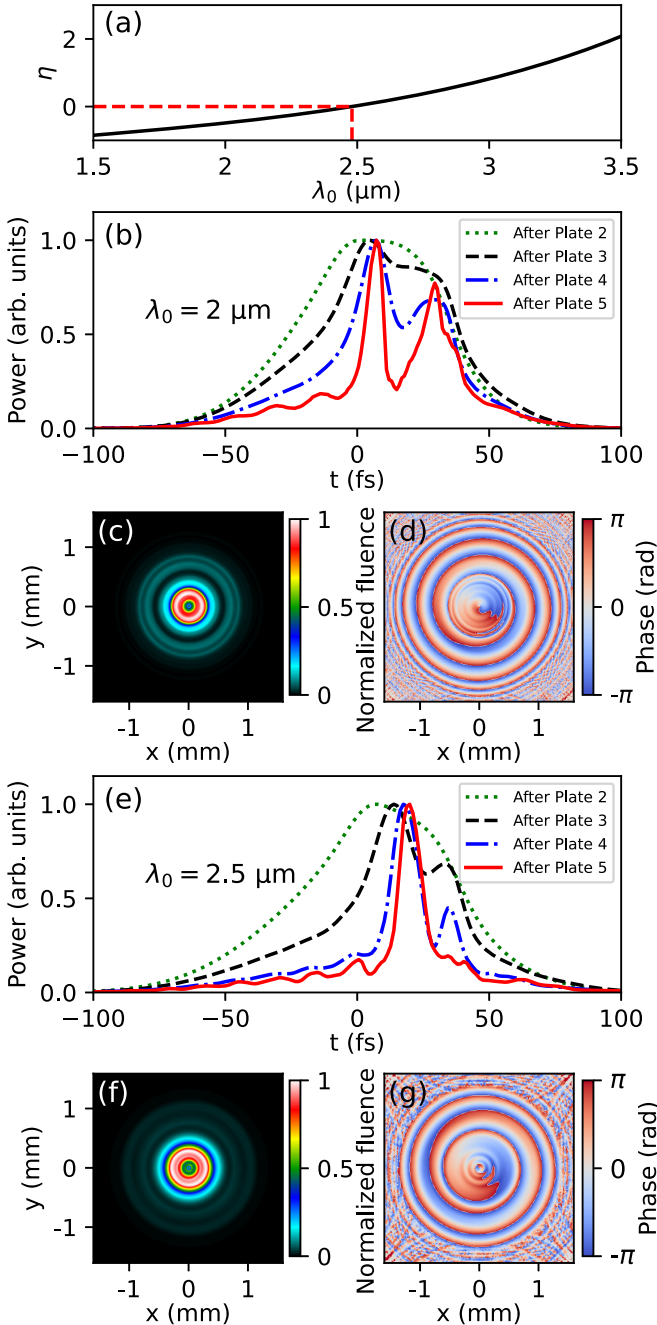


FIG. 1. (a) The evolution of η against λ_0 when we use the following settings: $n_2 = 2 \times 10^{-16} \text{ cm}^2/\text{W}$, $10 < I_0 < 20 \text{ (TW/cm}^2\text{)}$, and $\tau_0 = 9\lambda_0/c$. Numerical results for the self-compression of the femtosecond vortex beam with (b)–(d) $\lambda_0 = 2 \text{ }\mu\text{m}$ and $\tau_0 = 60 \text{ fs}$ and (e)–(g) $\lambda_0 = 2.5 \text{ }\mu\text{m}$ and $\tau_0 = 75 \text{ fs}$. The pulse energy is 3 mJ; five 300- μm -thick plates are used, and their spacings are varied to optimize the results. (b) and (e) The temporal power distribution of the pulse after each plate. (c) and (f) The fluence distribution of the output pulses. (d) and (g) Phase distribution of the output pulses.

$R(t) = (1 - \alpha)\delta(t) + \alpha\Theta(t)\frac{1 + \omega_R^2\tau_R^2}{\omega_R\tau_R}e^{-t/\tau_R}\sin(\omega_R t)$ contains an instantaneous contribution and a Raman-delayed contribution, with the ratio $\alpha = 0.18$ for silica and 0.5 for air. $\omega_R^{-1} = 12.2 \text{ fs}$ and $\tau_R = 32 \text{ fs}$ for fused silica, and $\omega_R^{-1} = 62.5 \text{ fs}$ and $\tau_R = 70 \text{ fs}$ for air. $\delta(t)$ is the delta function, and $\Theta(t)$ is the positive

unity function. The dispersion operator $\hat{D} = \sum_{n \geq 2} \binom{k^{(n)}}{n!} (i\partial_t)^n$ is calculated from the derivatives $k^{(n)} = \partial^n k / \partial \omega^n|_{\omega_0}$. The dispersion relations of fused silica and air are taken from [35,36] and are applicable to the simulated MIR range. The ionization potential $U_i = 9 \text{ eV}$ for fused silica and 12.1 eV for air. ρ_c is the critical plasma density, ρ_{nt} is the neutral species density, and τ_{rec} is the electron recombination time [33]. The ionization rate $W(|E|)$ for air is calculated from the Perelomov-Popov-Terent'ev model [34,37], and for fused silica we use the Keldysh rate [38].

The initial field is a singly charged Laguerre-Gaussian beam:

$$E(r, \varphi, t, z = 0) = E_0 \frac{r}{w} e^{-r^2/2w^2} e^{i\varphi} e^{-t^2/0.72\tau_0^2} e^{-ik_0 r^2/2f}, \quad (10)$$

where the beam radius $w = 200 \text{ }\mu\text{m}$, the focal length of the lens $f = 0.3 \text{ m}$, φ is the azimuthal angle, and the pulse energy is 3 mJ. The pulse duration (FWHM) τ_0 is nine optical cycles, 60 fs for $\lambda_0 = 2 \text{ }\mu\text{m}$, 75 fs for $\lambda_0 = 2.5 \text{ }\mu\text{m}$, and 90 fs for $\lambda_0 = 3 \text{ }\mu\text{m}$ to be specific. A 10% random amplitude perturbation is introduced to the initial field.

For all three wavelengths we use five 300- μm -thick fused silica plates, whose spacings are varied to make the incident intensity satisfy inequality (1). Note that in practice we can change both the thicknesses and spacings of the plates, which provides a wide parameter space. If $L < l_{\text{nl}}$, the spectrum of the output pulse is not sufficiently broadened; thus, the pulse cannot be compressed to a few cycles. If $L > 5l_{\text{nl}}$, the larger nonlinear phase accumulated in the hot spots will distort the vortex phase.

III. RESULTS AND DISCUSSION

First, we present the pulse compression results for $\lambda_0 = 2$ and 2.5 μm . When $\lambda_0 = 2 \text{ }\mu\text{m}$, the pulse is compressed in the first three plates, but pulse splitting occurs after the fourth plate [Fig. 1(b)], as expected. The formation of two subpulses is harmful to the temporal quality of the few-cycle pulse. As far as we simulated, changing the setting of the thin-plate system cannot fix this situation because the condition for the generation of the few-cycle vortex beam [inequality (7)] cannot be satisfied for this wavelength, and in this case, the negative dispersion of the material cannot compensate for the positive chirp induced by SPM. For $\lambda_0 = 2.5 \text{ }\mu\text{m}$ [Fig. 1(e)], pulse splitting is also observed after the third plate. However, in this case the latter subpulse is gradually arrested by the more intense pulse, leading to a single pulse in the end. This is because the negative dispersion is stronger for $\lambda_0 = 2.5 \text{ }\mu\text{m}$, and the blueshift part of the latter subpulse can catch up with the leading part. The fusion of the two subpulses leads to a single pulse with an obvious pedestal in the leading and tailing parts. As for the spatial characteristics, for both cases we can see that the fluence has a concentric ring structure [Figs. 1(c) and 1(f)], and the spiral phase profile is preserved [Figs. 1(d) and 1(g)]. The above results verify our theoretical analysis. We note that our theory aims at the choice of the central wavelength, and we take into account only second-order dispersion and SPM. This approximation neglects the influence of high-order dispersion, ionization, and the change in pulse duration, which leads to a small deviation when λ_0

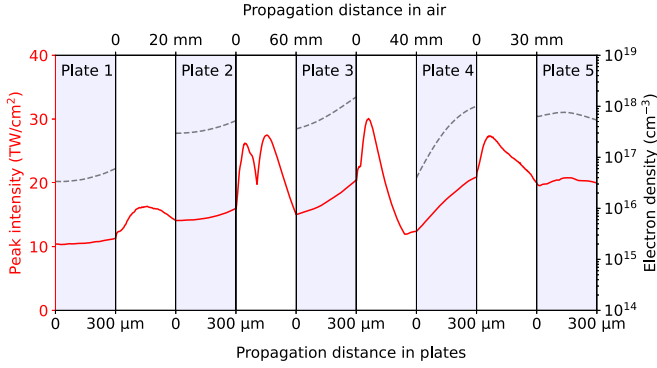


FIG. 2. Evolution of peak intensity (solid lines) and electron density (dashed lines) solved from Eqs. (8) and (9). The input vortex pulse has a duration of 90 fs and energy of 3 mJ, with central wavelength $\lambda_0 = 3 \mu\text{m}$. Five 300- μm -thick fused silica plates (colored area) are used to generate few-cycle vortex beams. The spacings between adjacent plates (air gap denoted by white area) are 20, 60, 40, and 30 mm.

is close to the critical value of $2.48 \mu\text{m}$. In spite of this, our analysis offers useful guidance for the experiment. We can expect that for a longer wavelength like $3 \mu\text{m}$, pulse splitting may be entirely circumvented, and few-cycle vortex beams with high temporal quality can be obtained, which will be discussed in detail in the following paragraphs.

We start with an overall view of the propagation process for a laser pulse with $\lambda_0 = 3 \mu\text{m}$. The evolution curves of peak intensity and electron density are shown in Fig. 2. Although there is a noticeable increase in the peak intensity in each plate, the intensity varies between 10 and 20 TW/cm^2 , which will not damage the plate but is high enough to trigger spectral broadening. The obvious increase in intensity in each plate is caused by the temporal compression of the pulse, as will be discussed further below. After each plate, the vortex beam refocuses in air, leading to the rapid increase in intensity. This phenomenon was investigated in detail for a Gaussian beam, where the nonlinear phase accumulated in the fused silica acts as an effective lens, making the beam refocus in air [33]. During the whole propagation process, the electron density is kept at a relatively low level in the plates ($< 2 \times 10^{18} \text{cm}^{-3}$) and is negligible ($< 10^{14} \text{cm}^{-3}$) in air. The relatively low intensity and electron density slow the growth of the modulation instability and inhibit multifilamentation, so that the characteristics of the vortex are retained during pulse compression [20].

After propagation in the five plates, the pulse is compressed to 15.1 fs, which is about 1.5 optical cycles, with the spectrum spanning from 2 to 4 μm , as shown in Figs. 3(a) and 3(b). Moreover, this few-cycle pulse keeps the ring-shaped intensity distribution with a central singularity in the transverse plane, like the initial distribution, as shown in Figs. 3(c) and 3(e). The spiral phase profile in Fig. 3(f) indicates that this few-cycle pulse keeps the same topological charge as the initial laser pulse [Fig. 3(d)]. These results suggest that we obtain a few-cycle vortex beam via self-compression of the MIR femtosecond vortex beam in the thin plates. Due to the low ionization loss in the scheme, this few-cycle vortex beam has an output energy of 2.75 mJ, corresponding to peak power of 0.18 TW and a high conversion efficiency of 91.5%.

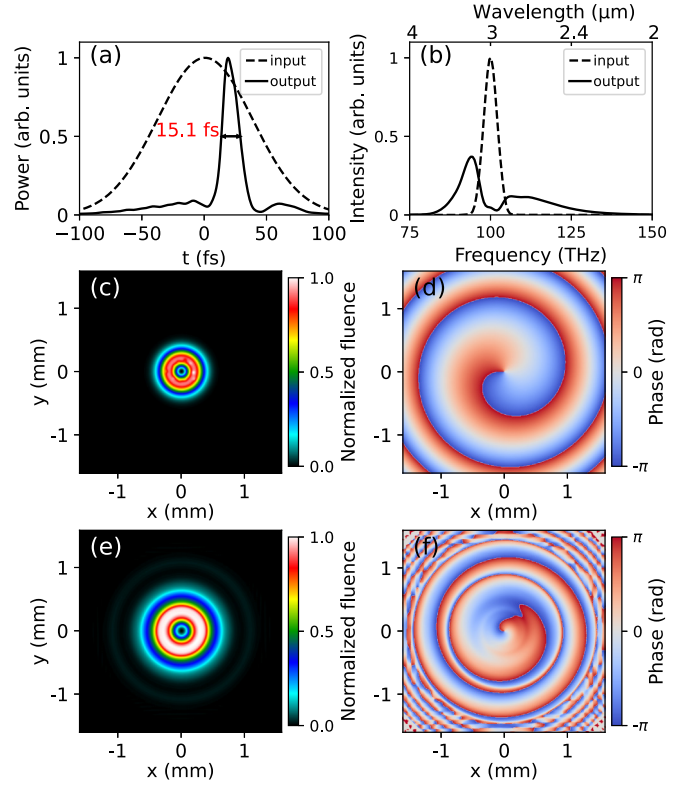


FIG. 3. (a) Pulse shape of the input (dashed line) and output (solid line) pulses. (b) Spectrum of the input (dashed line) and output (solid line) pulses. (c) The transverse fluence and (d) phase distribution of the input pulse. (e) The transverse fluence and (f) phase distribution of the output pulse. The time slice of the phase distribution corresponds to the intensity maximum. ($\lambda_0 = 3 \mu\text{m}$, $\tau_0 = 90 \text{fs}$, pulse energy is 3 mJ, and five 300- μm -thick plates are used.)

To investigate the generation mechanism of the few-cycle vortex beam, we plot the spectra and pulse profiles after each plate, as shown in Fig. 4. At first, we see a symmetric broadening of the spectrum, indicating that SPM is predominant in the first plate. Starting from plate 2, the spectrum extends to the blue side obviously. This is because of the frequency shift induced by SPM and ionization, which can be described by $\Delta\omega/\Delta z \propto \partial_t \rho(r, t)/2n_0\rho_c - n_2\partial_t I(r, t)$, where the first term has the same magnitude as the second term. Although the electron density is not high, the small value of ρ_c makes SPM and ionization both contribute greatly to spectrum broadening. After five plates, an octave-spanning spectrum that spans from 2 to 4 μm is obtained. The evolution of the pulse profiles in Fig. 4(b) shows that the pulse undergoes remarkable compression in the plates due to strong negative GDD. The 90-fs input-pulse duration is gradually compressed to 15.1 fs after five plates. Note that during the compression, no obvious steep tailing edge is observed, and a quantitative analysis is given below. The Kerr effect makes the refractive index of the pulse peak higher than that of the pulse leading edge, given by $\Delta n = n_{\text{peak}} - n_{\text{lead}} = n_2\Delta I$, which shifts the pulse peak towards the tailing edge at $t > 0$. The relative delay of the pulse peak and leading edge is thus given by $\Delta t_{\text{Kerr}} = \Delta z/v_{\text{peak}} - \Delta z/v_{\text{lead}} = \Delta n\Delta z/c$, where Δz is the propagation distance. Similarly,

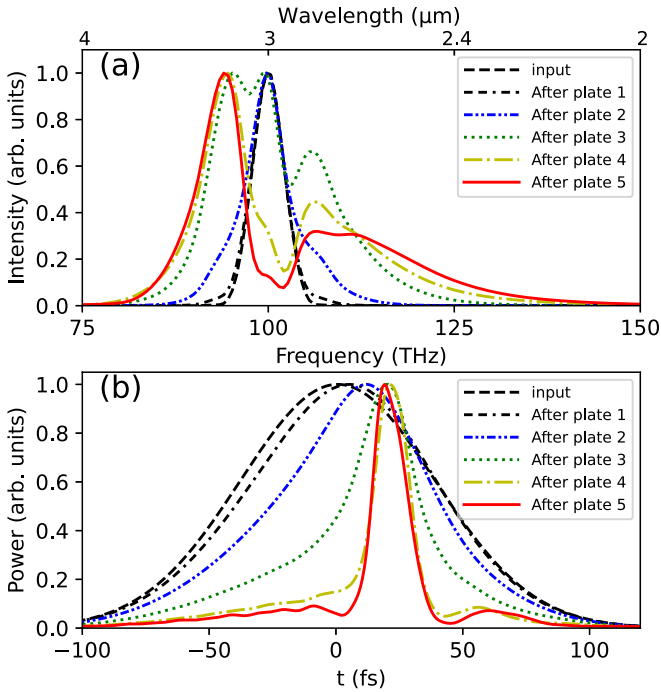


FIG. 4. (a) Spectra and (b) temporal power distribution of the laser pulse after each plate. The spectra and power are integrated over the whole transverse plane. The pulse durations after each plate are 85.3, 67.6, 31.2, 16.2, and 15.1 fs, respectively. ($\lambda_0 = 3 \mu\text{m}$, $\tau_0 = 90$ fs, pulse energy is 3 mJ, and five 300- μm -thick plates are used.)

the GDD-induced delay time of the pulse peak and leading edge is estimated to be $\Delta t_{\text{GDD}} = 2\pi k^{(2)} \Delta f \Delta z$, where $k^{(2)} = -534 \text{ fs}^2/\text{mm}$ for fused silica at $3 \mu\text{m}$, and Δf is the central frequency difference of the pulse peak and leading edge. Assuming $\Delta I = 10 \text{ TW}/\text{cm}^2$, $\Delta f = 20 \text{ THz}$, and $\Delta z = 1 \text{ mm}$, we get $\Delta t_{\text{Kerr}} = 6.7 \text{ fs}$ and $\Delta t_{\text{GDD}} = -67 \text{ fs}$. Since $|\Delta t_{\text{GDD}}|$ is much larger than $|\Delta t_{\text{Kerr}}|$, self-compression induced by GDD is more significant than self-steepening induced by SPM. As the pulse tailing edge becomes steep, the pulse leading edge is also compressed rapidly towards the tailing edge. Consequently, both the leading and tailing edges become steep in the output few-cycle pulse; thus, the traditional self-steepening effect is not obvious here. Meanwhile, this leads to soliton-like self-compression without pulse splitting, which enables a higher compression ratio and better temporal quality with a low-intensity pedestal.

In Fig. 5 we give a dynamic view of how the chirp is compensated via the GDD of plates. We select two spectral regions, the red-side component (RSC; $\lambda > 3.2 \mu\text{m}$) and the blue-side component (BSC; $\lambda < 2.8 \mu\text{m}$). For each spectral component, we filter it and perform an inverse Fourier transform to get its wave packet in the time domain. Figure 5 shows the temporal distribution of the two components at the front surface and back surface of each plate. Due to SPM, the RSC and BSC are located symmetrically at the back surface of the first plate, with RSC in the pulse leading edge and BSC in the tailing edge. Although ionization also contributes greatly to the spectral broadening in the following plates, the temporal distribution of the BSC is not obviously distorted, and only the

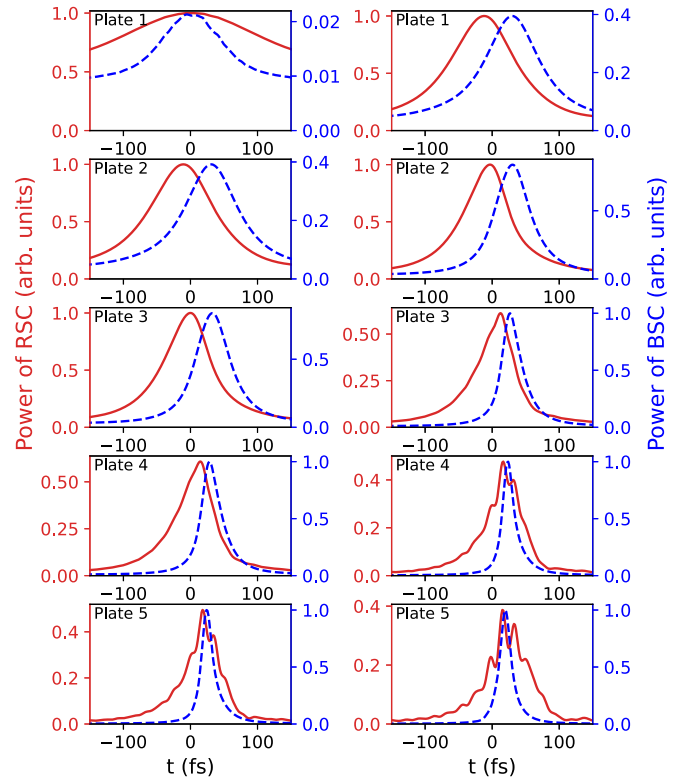


FIG. 5. Power distribution of the red-side component (RSC; $\lambda > 3.2 \mu\text{m}$; solid lines) and blue-side component (BSC; $\lambda < 2.8 \mu\text{m}$; dashed lines) in the temporal region for the front surface (left column) and back surface (right column) of each plate. Both components are filtered from the spectra of the vortex beam before and after each plate and are inversely Fourier transformed to get temporal profiles. ($\lambda_0 = 3 \mu\text{m}$, $\tau_0 = 90$ fs, pulse energy is 3 mJ, and five 300- μm -thick plates are used.)

proportion of the BSC increases. With further propagation in plates and broadening of the spectrum [Fig. 4(a)], the effect of GDD becomes more significant. It can be seen that the RSC and BSC continuously draw close (right column in Fig. 5), which leads to the compression of the pulse. In addition, after plate 3 the duration of the BSC becomes much shorter than that of the RSC. This is in accordance with the extra spectral blueshift induced by ionization shown in Fig. 4. Finally, after plate 5, RSC and BSC are synchronized in time, and the pulse is compressed to 15.1 fs. Figure 5 also indicates that the propagation in air has little influence on pulse compression. However, the air gap is crucial to the inhibition of multifilamentation and retaining vortex characteristics, where the vortex beam undergoes a self-healing process of spatial distortions [20].

The influence of the spatial intensity distribution on pulse compression has also been investigated. In Fig. 6(a) we show the temporal intensity and phase of different transverse positions for the laser pulse after plate 5. Three typical transverse positions (inner ring, intensity maximum, and outer ring) are selected, marked by stars S1, S2, and S3 in the inset. For these three positions, the pulses are all compressed below 10 fs, and the pulse duration of S3 is larger, as we expect. This is because the periphery has a lower intensity and ex-

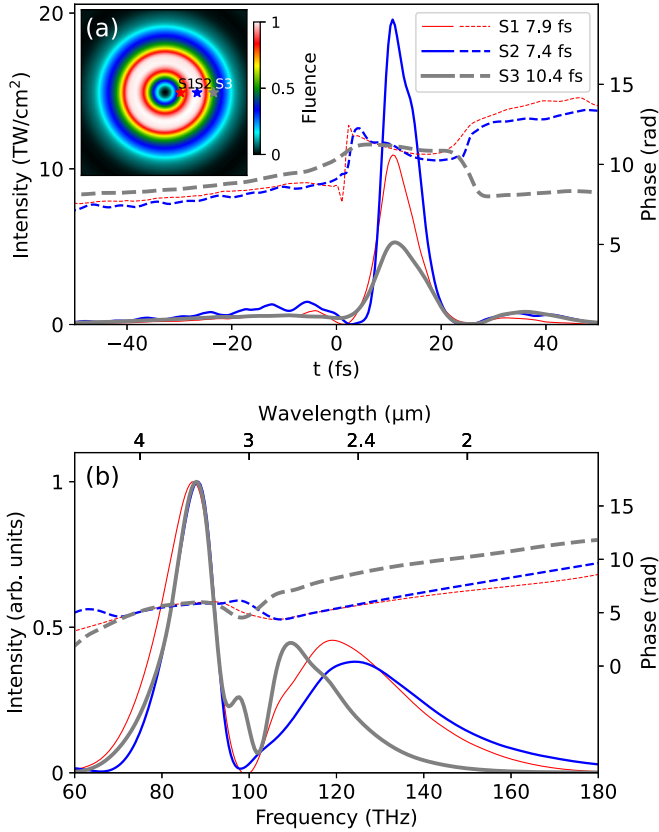


FIG. 6. (a) Temporal intensity (solid lines) and phase (dashed lines) of the laser pulse after plate 5 for three transverse positions (marked by stars in the inset: S1, $r = 0.16$ mm; S2, $r = 0.32$ mm; S3, $r = 0.48$ mm). (b) Spectral intensity (solid lines) and phase (dashed lines) of the laser pulse after plate 5 for the three transverse positions. Inset: the fluence distribution of the laser pulse after plate 5, the same as in Fig. 3(e). ($\lambda_0 = 3$ μm , $\tau_0 = 90$ fs, pulse energy is 3 mJ, and five 300- μm -thick plates are used.)

periences less spectrum broadening. We can also see that the temporal phase slope of S2 is higher than those of S1 and S3, indicating that S2 has more blueshift spectral components due to stronger ionization. The above explanation is further verified by Fig. 6(b), where we show the corresponding spectral intensity and phase. As we can see, due to SPM and ionization, the fundamental wavelength (3 μm) almost disappears, and there are two peaks in the redshift (>3 μm) and blueshift (<3 μm) regions. In the main peak of the spectra (3.24–3.75 μm), the three spectral phase curves are all flat, which means the chirp is sufficiently compensated. For the blueshift region, the spectrum of S2 has a broader extension to the blue side with a larger positive chirp, which also indicates that S2 has stronger ionization. In addition, since the uncompressed portion mainly locates at the periphery, a spatial filtering technique may be used to obtain shorter pulses.

Energy scaling is also an important criterion when evaluating pulse-compression schemes, especially for the study of HHG, for which a high-energy few-cycle pulse is preferred. To further increase the power of the MIR few-cycle vortex beam obtained by using the thin-plate scheme, two main aspects have to be considered: avoiding multiple filamentation and damage to the fused silica plates and avoiding beam collapse in air gaps. For the former challenge, the high-energy beam could be expanded to have a larger diameter, which can maintain the high intensity while avoiding multiple filamentation and material damage. For the latter problem, the thin-plate system can be put in a cell filled with low-pressure gas or even vacuum to reduce or eliminate the nonlinearity of the gaps. The above suggested solutions further guarantee that the thin-plate scheme is a promising method to generate MIR few-cycle vortex beams with high energy.

IV. CONCLUSION

The thin-plate scheme is supposed to be a promising solution for obtaining high-energy few-cycle vortex beams by self-compression of the femtosecond vortex beam. We theoretically gave the criteria for choosing the parameters of the plates and laser wavelength. Our analysis is based on the assumption of proper spatiotemporal matching. That is, the spectrum is broadened enough, the negative dispersion can compensate for the positive chirp induced by nonlinear effects, and multiple filamentation is avoided. The theoretical analysis is further verified by simulation. We numerically investigated the self-compression of a 3- μm femtosecond vortex beam. Due to the strong negative dispersion of the fused silica plates, the femtosecond vortex beam undergoes solitonlike pulse self-compression, and the pulse is compressed from 3 mJ/90 fs to 2.75 mJ/15.1 fs, corresponding to about 1.5 optical cycles with a peak power of 0.18 TW. At the same time, the thin-plate scheme prevents destructive multifilamentation, so that the few-cycle pulse preserves the vortex characteristics. As a result, a few-cycle vortex beam is obtained, and the conversion efficiency is as high as 91.5% due to weak ionization. Our work is instructive for future experiments and will benefit the generation of isolated attosecond light vortices, opening an alternative perspective in ultrafast science.

ACKNOWLEDGMENTS

This work was supported by the National Natural Science Foundation of China (Grants No. 11874056, No. 12074228, and No. 11774038), the Natural Science Foundation of Shandong Province (Grant No. ZR2021MA023), the Taishan Scholar Project of Shandong Province (Grant No. tsqn201812043), and the Innovation Group of Jinan (Grant No. 2020GXRC039).

[1] Y. Shen, X. Wang, Z. Xie, C. Min, X. Fu, Q. Liu, M. Gong, and X. Yuan, Optical vortices 30 years on: OAM manipulation from topological charge to multiple singularities, *Light Sci.: Appl.* **8**, 90 (2019).

[2] R. Fickler, G. Campbell, B. Buchler, P. K. Lam, and A. Zeilinger, Quantum entanglement of angular momentum states with quantum numbers up to 10,010, *Proc. Natl. Acad. Sci. USA* **113**, 13642 (2016).

- [3] S. Franke-Arnold, L. Allen, and M. Padgett, Advances in optical angular momentum, *Laser Photonics Rev.* **2**, 299 (2008).
- [4] N. Jhajj, I. Larkin, E. W. Rosenthal, S. Zahedpour, J. K. Wahlstrand, and H. M. Milchberg, Spatiotemporal Optical Vortices, *Phys. Rev. X* **6**, 031037 (2016).
- [5] P. Hansinger, G. Maleshkov, I. L. Garanovich, D. V. Skryabin, D. N. Neshev, A. Dreischuh, and G. G. Paulus, Vortex algebra by multiply cascaded four-wave mixing of femtosecond optical beams, *Opt. Express* **22**, 11079 (2014).
- [6] Y. Fang, M. Han, P. Ge, Z. Guo, X. Yu, Y. Deng, C. Wu, Q. Gong, and Y. Liu, Photoelectronic mapping of the spin-orbit interaction of intense light fields, *Nat. Photonics* **15**, 115 (2021).
- [7] M. Zürch, C. Kern, P. Hansinger, A. Dreischuh, and C. Spielmann, Strong-field physics with singular light beams, *Nat. Phys.* **8**, 743 (2012).
- [8] G. Gariepy, J. Leach, K. T. Kim, T. J. Hammond, E. Frumker, R. W. Boyd, and P. B. Corkum, Creating High-Harmonic Beams with Controlled Orbital Angular Momentum, *Phys. Rev. Lett.* **113**, 153901 (2014).
- [9] F. Kong, C. Zhang, F. Bouchard, Z. Li, G. G. Brown, D. H. Ko, T. Hammond, L. Arissian, R. W. Boyd, E. Karimi, and P. B. Corkum, Controlling the orbital angular momentum of high harmonic vortices, *Nat. Commun.* **8**, 14970 (2017).
- [10] L. Rego, K. M. Dorney, N. J. Brooks, Q. L. Nguyen, C.-T. Liao, J. San Roman, D. E. Couch, A. Liu, E. Pisanty, M. Lewenstein, L. Plaja, H. C. Kapteyn, M. M. Murnane, and C. Hernández-García, Generation of extreme-ultraviolet beams with time-varying orbital angular momentum, *Science* **364**, eaaw9486 (2019).
- [11] R. Géneaux, A. Camper, T. Auguste, O. Gobert, J. Caillat, R. Taïeb, and T. Ruchon, Synthesis and characterization of attosecond light vortices in the extreme ultraviolet, *Nat. Commun.* **7**, 12583 (2016).
- [12] R. Kerber, J. Fitzgerald, S. Oh, D. Reiter, and O. Hess, Orbital angular momentum dichroism in nanoantennas, *Commun. Phys.* **1**, 87 (2018).
- [13] A. Picón, J. Mompart, J. V. de Aldana, L. Plaja, G. Calvo, and L. Roso, Photoionization with orbital angular momentum beams, *Opt. Express* **18**, 3660 (2010).
- [14] A. Picón, A. Benseny, J. Mompart, J. V. de Aldana, L. Plaja, G. F. Calvo, and L. Roso, Transferring orbital and spin angular momenta of light to atoms, *New J. Phys.* **12**, 083053 (2010).
- [15] R. Cireasa, A. E. Boguslavskiy, B. Pons, M. C. H. Wong, D. Descamps, S. Petit, H. Ruf, N. Thiré, A. Ferré, J. Suarez, J. Higué, B. E. Schmidt, A. F. Alharbi, F. Légaré, V. Blanchet, B. Fabre, S. Patchkovskii, O. Smirnova, Y. Mairesse, and V. R. Bhardwaj, Probing molecular chirality on a sub-femtosecond timescale, *Nat. Phys.* **11**, 654 (2015).
- [16] G. Sansone, E. Benedetti, F. Calegari, C. Vozzi, L. Avaldi, R. Flammini, L. Poletto, P. Villoresi, C. Altucci, R. Velotta, S. Stagira, S. D. Silvestri, and M. Nisoli, Isolated single-cycle attosecond pulses, *Science* **314**, 443 (2006).
- [17] H. Wang, Q. Song, S. Zheng, Q. Lin, E. Wu, Y. Ai, C. Liu, and S. Xu, Terahertz-mid-infrared anisotropic vortex beams generation via few-cycle vortex-laser-induced air plasma, *J. Opt.* **21**, 095501 (2019).
- [18] K. Yamane, Y. Toda, and R. Morita, Ultrashort optical-vortex pulse generation in few-cycle regime, *Opt. Express* **20**, 18986 (2012).
- [19] X.-L. Zhu, M. Chen, S.-M. Weng, P. McKenna, Z.-M. Sheng, and J. Zhang, Single-Cycle Terawatt Twisted-Light Pulses at Midinfrared Wavelengths Above 10 μm , *Phys. Rev. Appl.* **12**, 054024 (2019).
- [20] L. Xu, D. Li, J. Chang, D. Li, T. Xi, and Z. Hao, Powerful supercontinuum vortices generated by femtosecond vortex beams with thin plates, *Photonics Res.* **10**, 802 (2022).
- [21] M. Seo, K. Tsendsuren, S. Mitra, M. Kling, and D. Kim, High-contrast, intense single-cycle pulses from an all thin-solid-plate setup, *Opt. Lett.* **45**, 367 (2020).
- [22] N. L. Wagner, E. A. Gibson, T. Popmintchev, I. P. Christov, M. M. Murnane, and H. C. Kapteyn, Self-Compression of Ultrashort Pulses through Ionization-Induced Spatiotemporal Reshaping, *Phys. Rev. Lett.* **93**, 173902 (2004).
- [23] G. C. Nagar and B. Shim, Study of wavelength-dependent pulse self-compression for high intensity pulse propagation in gas-filled capillaries, *Opt. Express* **29**, 27416 (2021).
- [24] D. N. Neshev, A. Dreischuh, G. Maleshkov, M. Samoc, and Y. S. Kivshar, Supercontinuum generation with optical vortices, *Opt. Express* **18**, 18368 (2010).
- [25] T. Popmintchev, M.-C. Chen, D. Popmintchev, P. Arpin, S. Brown, S. Ališauskas, G. Andriukaitis, T. Balčiūnas, O. D. Mücke, A. Pugžlys, A. Baltuška, B. Shim, S. E. Schrauth, A. Gaeta, C. Hernández-García, L. Plaja, A. Becker, A. Jaron-Becker, M. M. Murnane, and H. C. Kapteyn, Bright coherent ultrahigh harmonics in the keV x-ray regime from mid-infrared femtosecond lasers, *Science* **336**, 1287 (2012).
- [26] J. Weisshaupt, V. Juvé, M. Holtz, S. Ku, M. Woerner, T. Elsaesser, S. Ališauskas, A. Pugžlys, and A. Baltuška, High-brightness table-top hard x-ray source driven by sub-100-femtosecond mid-infrared pulses, *Nat. Photonics* **8**, 927 (2014).
- [27] C.-H. Lu, Y.-J. Tsou, H.-Y. Chen, B.-H. Chen, Y.-C. Cheng, S.-D. Yang, M.-C. Chen, C.-C. Hsu, and A. H. Kung, Generation of intense supercontinuum in condensed media, *Optica* **1**, 400 (2014).
- [28] Y.-C. Cheng, C.-H. Lu, Y.-Y. Lin, and A. Kung, Supercontinuum generation in a multi-plate medium, *Opt. Express* **24**, 7224 (2016).
- [29] J. Qian, Y. Peng, Y. Li, B. Shao, Z. Liu, W. Li, R. Feng, L. Shen, Y. Leng, and R. Li, Few-cycle mid-infrared laser based on nonlinear self-compression in solid thin plates, *Opt. Lett.* **46**, 5075 (2021).
- [30] A. A. Voronin and A. M. Zheltikov, Pulse self-compression to single-cycle pulse widths a few decades above the self-focusing threshold, *Phys. Rev. A* **94**, 023824 (2016).
- [31] G. P. Agrawal, in *Applications of Nonlinear Fiber Optics*, edited by G. P. Agrawal (Academic, San Diego, 2001).
- [32] G. N. Patwardhan, J. S. Ginsberg, C. Y. Chen, M. M. Jadidi, and A. L. Gaeta, Nonlinear refractive index of solids in mid-infrared, *Opt. Lett.* **46**, 1824 (2021).
- [33] L. Bergé, S. Skupin, and G. Steinmeyer, Self-recompression of laser filaments exiting a gas cell, *Phys. Rev. A* **79**, 033838 (2009).
- [34] L. Bergé, S. Skupin, R. Nuter, J. Kasparian, and J.-P. Wolf, Ultrashort filaments of light in weakly ionized, optically transparent media, *Rep. Prog. Phys.* **70**, 1633 (2007).

- [35] C. Tan, Determination of refractive index of silica glass for infrared wavelengths by ir spectroscopy, *J. Non-Cryst. Solids* **223**, 158 (1998).
- [36] R. J. Mathar, Refractive index of humid air in the infrared: Model fits, *J. Opt. A* **9**, 470 (2007).
- [37] A. M. Perelomov, V. S. Popov, and M. V. Terent'ev, Ionization of atoms in an alternating electric field, *Zh. Eksp. Teor. Fiz.* **50**, 1393 (1966) [*Sov. Phys. JETP* **23**, 924 (1966)].
- [38] L. Keldysh, Ionization in the field of a strong electromagnetic wave, *Zh. Eksp. Teor. Fiz.* **47**, 1945 (1965) [*Sov. Phys. JETP* **20**, 1307 (1965)].